JUSTC

Article

http://justc.ustc.edu.cn

Received: September 30, 2024; Accepted: December 03, 2024

Quantitative analysis of the ohmic resistance in aqueous organic redox flow batteries

Kang Peng, Junkai Fang, Siyu Chen, Peipei Zuo, Tongwen Xu, and Zhengjin Yang ✉

State Key Laboratory of Precision and Intelligent Chemistry, Department of Applied Chemistry, School of Chemistry and Materials Science, University of Science and Technology of China, Hefei 230026, China

✉Correspondence: Zhengjin Yang, E-mail: yangzj09@ustc.edu.cn

Graphical abstract

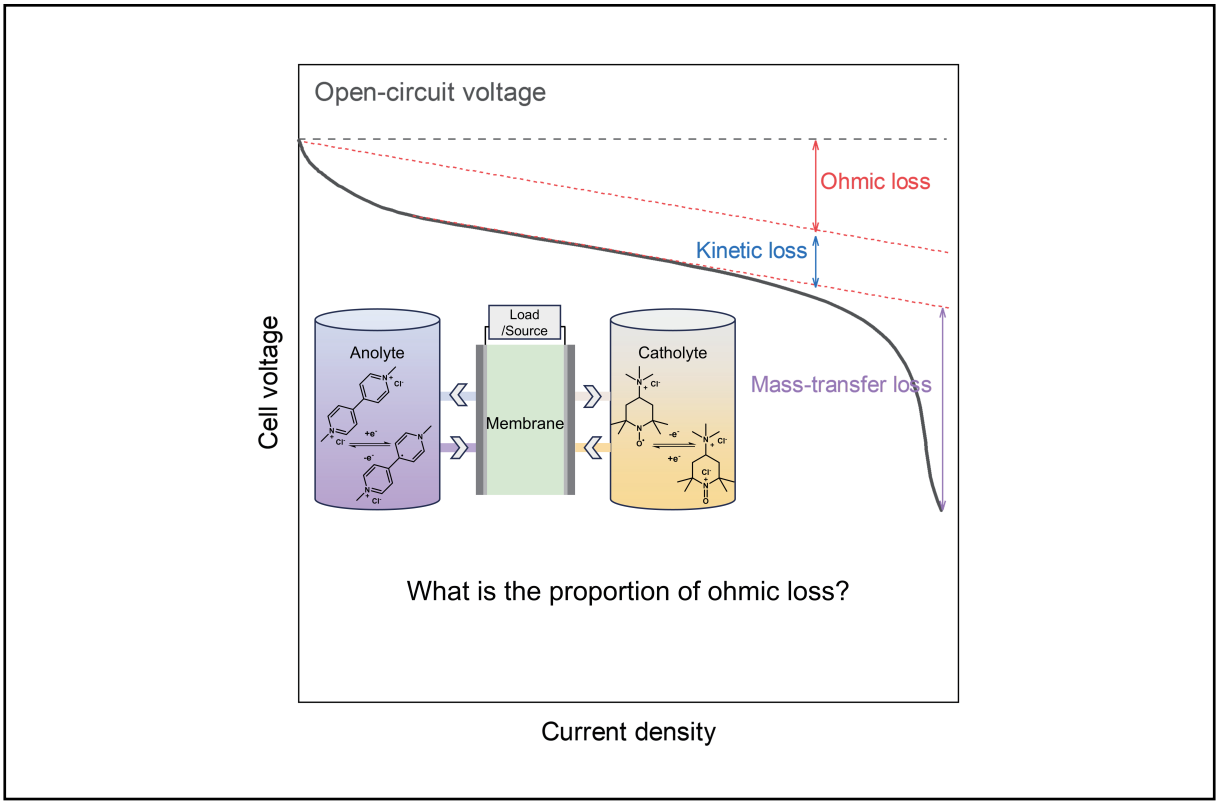

In the TEMPTMA/MV cell, electrochemical impedance spectroscopy studies and cell polarization are conducted to determine the proportion of the ohmic resistance.

Public summary

- Comprehensive electrochemical impedance spectroscopy studies and cell polarization are conducted on a representative TEMPTMA/MV cell assembled with a commercial AMVN membrane.
- The proportions of the ohmic resistance to the total cell resistance at various stages of charge ranging from 10% to 100% are quantitatively analyzed.
- The determination of the major contributors to cell resistance provides insight into the development of high-power-density aqueous organic redox flow batteries.

Citation: Peng K, Fang J K, Chen S Y, et al. Quantitative analysis of the ohmic resistance in aqueous organic redox flow batteries. *JUSTC*, **2025**, 55(6): 0603. CSTR: 32290.14.JUSTC-2024-0129. DOI: 10.52396/JUSTC-2024-0129

JUSTC

Article

http://justc.ustc.edu.cn

Received: September 30, 2024; Accepted: December 03, 2024

Quantitative analysis of the ohmic resistance in aqueous organic redox flow batteries

Kang Peng, Junkai Fang, Siyu Chen, Peipei Zuo, Tongwen Xu, and Zhengjin Yang ✉

State Key Laboratory of Precision and Intelligent Chemistry, Department of Applied Chemistry, School of Chemistry and Materials Science, University of Science and Technology of China, Hefei 230026, China

✉Correspondence: Zhengjin Yang, E-mail: yangzj09@ustc.edu.cn

Cite This: *JUSTC*, **2025**, 55(6): 0603 (5pp)

Read Online

Abstract: Aqueous organic redox flow batteries (AORFBs) exploit the reversible electrochemical reactions of water-soluble organic redox-active species to store electricity and have emerged as promising electrochemical energy storage technologies. To improve the battery performance related to the cell resistance, such as the power density and energy efficiency, it is essential to understand the cell resistance and determine the major contributor. Here, we conduct comprehensive electrochemical impedance spectroscopy (EIS) studies and cell polarization on a representative TEMPTMA/MV cell assembled with a commercial AMVN membrane and probe the proportion of the ohmic resistance to the total cell resistance at various stages of charge (SOCs) ranging from 10% to 100%. At 0 mA·cm^{-2}, the ohmic resistance is responsible for 60.3%–71.7% of the resistance of the entire cell, whereas at high current densities (for example, when the power density reaches the maximum), the ohmic resistance still contributes 47.9%–61.4%. Our quantitative analysis highlights the dominance of the ohmic resistance and anticipates that a membrane with lower resistivity may significantly increase the power density.

Keywords: aqueous organic redox flow battery; ohmic resistance; electrochemical impedance spectroscopy; cell polarization; power density

CLC number: TM912 **Document code:** A

1 Introduction

With rapidly decreasing costs and fast-improving technology maturity, the deployment of grid-integrated renewable sources of energy, such as solar and wind power, has accelerated greatly in recent years[1–3]. However, renewable sources of energy are intrinsically intermittent, impeding their widespread application in large-scale power production[4,5]. This conundrum may be solved by aqueous redox flow batteries[6], which store electrical energy with low-cost and nonflammable electrolytes in external tanks, thereby decoupling power and energy. The output power (kW) is controlled by the cell stacks, whereas the energy capacity (kW·h) is set by the electrolyte tanks[7]. This spatial decoupling can be leveraged to realize discharge durations from hours to days and smooth fluctuations in the renewable electricity supply[8].

Aqueous organic redox flow batteries (AORFBs) not only retain spatial decoupling but also exploit organic redox-active species with fast redox kinetics, high solubility, and easy scale production[9,10]. In the past ten years, extensive research efforts have been devoted to understanding the electrochemical behavior of organic redox-active species and their chemical stability during prolonged cell cycling[11], but only a limited number of studies have discussed the underlying sources of the power performance of AORFBs. Amini et al.[12] summarized the areal power densities reported for lab-scale redox flow batteries and critically evaluated the major pathway employed for power optimization: increasing the open circuit voltage (OCV) and reducing the area-specific resistance (ASR) of the cell. Increasing the OCV means widening the potential gap between the anolyte and catholyte via rational molecular engineering. For instance, Gao et al.[13] synthesized a pair of anionic organic molecules, namely, (PPBPy)Br_2 (1,1'-bis(3-phosphonopropyl)-4,4'-(1,4-phenylene) bispyridinium dibromide) and PSS-TEMPO (4-(propoxy-3-sodium sulfonate)-2,2,6,6-tetramethyl piperidin-1-yl)oxyl), which have a potential gap as high as 1.61 V and exhibited a record power density of 509 mW·cm^{-2} among all reported near-neutral AORFBs. Nevertheless, the OCV is beyond the water electrolysis onset voltage (> 1.3 V)[14], and side reactions (i.e., hydrogen evolution or oxygen evolution reactions) may severely occur. Reducing the cell ASR is therefore crucial. Zuo et al.[15] developed triazine framework membranes to achieve near-frictionless ion transport. The $K_4[Fe(CN)_6]$ (potassium ferrocyanide)/DHAQ (2,6-dihydroxyanthraquinone) cell with an equilibrium cell potential of 1.2 V could deliver a peak power density of 415 mW·cm^{-2}, with a low-resistance SCTF-BP membrane (0.17 Ω·cm^2). To understand this improvement in the peak power density, it is essential to understand the ratio of the ohmic resistance to the cell resistance and the effect of the cell resistance on the power performance.

For the typical AORFB polarization curve during discharging (Fig. 1), the potential losses due to charge transfer

CSTR: 32290.14.JUSTC-2024-0129
DOI: 10.52396/JUSTC-2024-0129
JUSTC, **2025**, 55(6): 0603

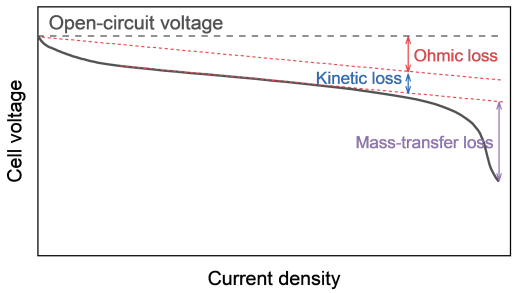

Fig. 1. Typical AORFB polarization curve during discharging with dissected contributions of ohmic, kinetic and mass-transfer losses.

(kinetic), ohmic, and concentration (mass-transfer) overpotentials are reflected[12]. The charge transfer and concentration overpotentials are significantly nonlinear and dependent on the current density. Nevertheless, the total cell resistance can be derived from the voltage–current curve[16]. Considering the measurement of the ohmic resistance via electrochemical impedance spectroscopy (EIS)[17,18] and the calculation of the power density via Ohm's law, the resistance and power issues of AORFBs can be quantitatively analyzed.

Herein, we conducted comprehensive EIS studies and cell polarization on a representative TEMPTMA (N,N,N-2,2,6,6-heptamethylpiperidinyl oxy-4-ammonium chloride)/MV (N,N'-dimethyl-4,4-bipyridinium dichloride) cell assembled with a commercial AMVN membrane[19,20]. The proportion of the ohmic resistance to the total cell resistance was probed at various stages of charge (SOCs) ranging from 10% to 100%. Specifically, the contributions of the ohmic resistance are 60.3%–71.7% at 0 mA·cm^{-2} and 47.9%–61.4% at high current densities. The derivation of the maximum power density suggested that a lower ohmic resistance may significantly increase the power density.

2 Materials and methods

2.1 Materials

N,N,N-2,2,6,6-heptamethylpiperidinyl oxy-4-ammonium chloride (TEMPTMA) and N,N'-dimethyl-4,4-bipyridinium dichloride (MV) were purchased from Suqian Time Energy Storage Technology Co., Ltd. (Suqian, China). The AMVN membrane was purchased from SCI Materials Hub. The complete specification of the AMVN membrane is "FORBLUE™ Selemion AMVN", which is a hydrocarbon-type anion exchange membrane developed and manufactured by the AGC Group. The thickness of the AMVN membrane is 100 μm. The chloridion transport number of the AMVN membrane is greater than 0.95. All the materials were used as received without further purification. Deionized (DI) water was utilized throughout the experiment.

2.2 Flow cell assembly

The flow cell hardware was purchased from Suqian Time Energy Storage Technology Co., Ltd. (Suqian, China). POCO sealed flow frames were used on both sides. The active area and depth of the flow frames were 7 cm×7 cm and 3 mm, respectively. The electrode on each side consisted of a sheet of carbon felt (baked at 400 °C for 24 h prior to use) with a 7 cm × 7 cm geometric area. The cell was assembled with a commercial AMVN membrane. After assembly, the cell was transferred to a glovebox with an oxygen concentration of < 2 ppm. The electrolytes were pumped through the cell stack at a flow volume rate of 140 mL·min^{-1} via a Masterfles L/S peristaltic pump (Cole-Parmer, Vernon Hills, IL).

2.3 EIS studies and cell polarizations

Cell polarization studies were performed on a Bio-Logic BCS-815 electrochemical workstation at room temperature. The polarization curves were obtained by charging the battery to a certain SOC, followed by polarizing by linear sweep voltammetry ranging between 0.5 V and 1.6 V. Potentio-controlled EIS in a frequency range from 1 Hz to 10 kHz was used to measure the cell resistance. For the TEMPTMA/MV cell (Fig. 2), the anolyte comprised 70 mL of 1.3 M MV, whereas the catholyte comprised 50 mL of 1.3 M TEMPTMA. The anolyte was 1.4 times e^- excess to ensure that the catholyte was the capacity limiting side.

3 Results and discussion

To charge the TEMPTMA (0.79 V vs. AgCl/Ag)/MV (−0.63 V vs. AgCl/Ag) cell stepwise with a 10% increase in the SOC, we first measured the total capacity of the cell via potentiostatic charge–discharge experiments with a cutoff current density of 4 mA·cm^{-2}[21]. The cell was charged to 6281 C at a constant voltage of 1.6 V (Fig. 3a) and exhibited a discharge capacity of 6198 C at 0.5 V (Fig. 3b), which is in accordance with its theoretical capacity of 6260 C (65 mmol e^-). The incremental capacity was then set to 620 C, and the cell was charged to various SOCs ranging from 10% to 100% (Fig. 3c).

With increasing SOC, the cell OCV gradually increases (Fig. 4a). This trend is consistent with the Nernst equation[22]. The Nernst equation calculates the potential of an electrochemical cell as follows.

$$E_{\text{cell}} = E^{\theta} - \frac{RT}{nF} \times \ln Q, \tag{1}$$

where E_{cell} is the cell potential, E^{θ} is the cell potential under standard conditions, R is the universal gas constant (8.314 J·mol^{-1}·K^{-1}), T is the temperature, n is the number of electrons transferred in the reaction, F is the Faraday constant (96485 C·mol^{-1}), and Q is the reaction quotient.

As the SOC increases, the Q of the discharge reaction decreases, thereby increasing the cell potential E_{cell}. That is,

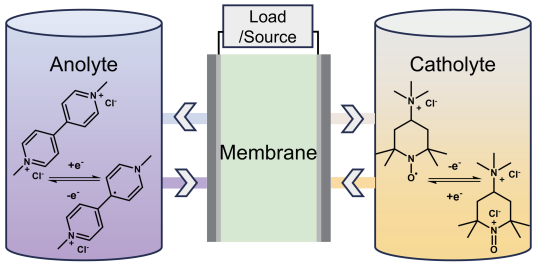

Fig. 2. Molecular structures of MV (the anolyte) and TEMPTMA (the catholyte) and their redox reactions at the electrode.

CSTR: 32290.14.JUSTC-2024-0129
DOI: 10.52396/JUSTC-2024-0129
JUSTC, **2025**, 55(6): 0603

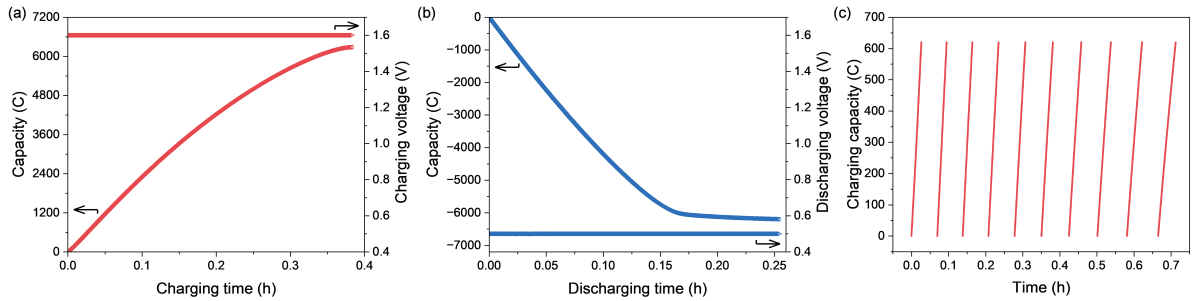

Fig. 3. (a) Charging and (b) discharging curves of the TEMPTMA/MV cell at constant voltages of 1.6 V and 0.5 V, respectively. (c) Stepwise charging curve of the TEMPTMA/MV cell at 1.6 V with a 10% increment in the state of charge (SOC).

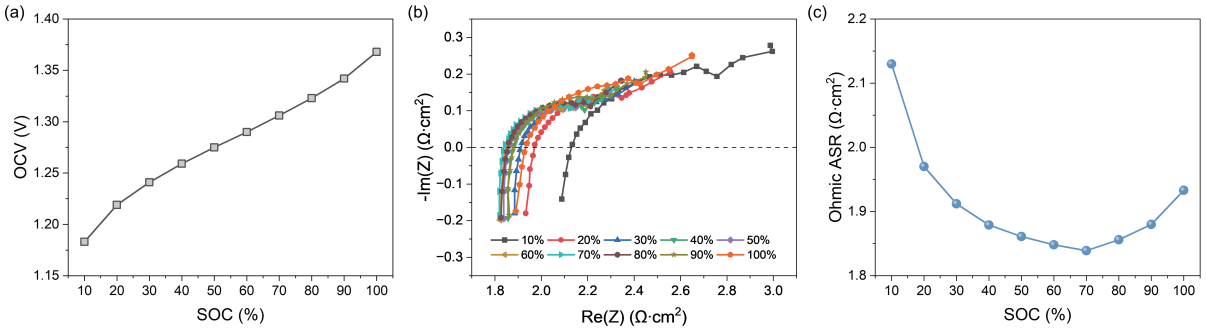

Fig. 4. (a) Open-circuit voltages (OCVs), (b) ohmic area-specific resistances (ASRs), and (c) electrochemical impedance spectroscopy (EIS) spectra of the TEMPTMA/MV cell at various SOCs.

the cell OCV increases as the SOC increases.

We conducted EIS studies to obtain the ohmic ASR values of the TEMPTMA/MV cell (Fig. 4b). The ohmic ASR includes the membrane, electrolyte, and electrode ASRs and is dictated by the intercept from the EIS spectrum on the dashed line[23]. Fig. 4c shows the ohmic ASR of the cell at various SOCs. With increasing SOC, the ohmic ASR first decreases but then increases. The increase may be attributed to the increase in the electrolyte viscosity because the singly reduced bipyridinium species (monoradicals) tend to aggregate through π–π stacking with a concentration-dependent average number of 1–6[24,25].

After the ohmic ASRs of the TEMPTMA/MV cell were measured, the polarization curves at various SOCs were studied (Fig. 5a). Owing to the strong dependence of the concentration polarization on the current density[26], we first evaluated the ratio of the ohmic resistance to the cell resistance at 0 mA·cm^{-2}. The derivatives of the polarization curves at 0 mA·cm^{-2} indicate the total-cell ASRs (Fig. 5b). The trend of the total cell ASR with the SOC is the same as that of the ohmic ASR with the SOC. At various SOCs ranging from 10% to 100%, the ohmic resistance is responsible for 60.3%–71.7% of the cell resistance (Fig. 5c).

At high current densities, the concentration polarization increases, and the proportion of the ohmic resistance decreases[27,28]. In addition, the concentration polarization becomes more pronounced toward the end of the charge and discharge phases, i.e., at high SOCs during charging and low SOCs during discharging[29]. To calculate the cell resistance at high current densities, power density data were extracted from polarization curves, as shown in Fig. 5d. The power density is affected by the cell resistance and current density[12]:

$$P = OCV \times i - R_{\text{cell}} \times i^2, \tag{2}$$

where P and i represent the cell's power density and current density, respectively, and R_{cell} is the total cell ASR.

At the point of the maximum power density (P_{max}), the current density is derived from taking the derivative of Eq. (2) with respect to the current density:

$$\frac{\mathrm{d}P}{\mathrm{d}i} = OCV - 2 \times R_{\text{cell}} \times i = 0, \tag{3}$$

$$i_{P_{\text{max}}} = \frac{OCV}{2 \times R_{\text{cell}}}, \tag{4}$$

where $i_{P_{\text{max}}}$ denotes the current density at the point P_{max}.

Substituting Eq. (4) into Eq. (2), the relationship between P_{max} and R_{cell} is as follows:

$$P_{\text{max}} = \frac{OCV^2}{4 \times R_{\text{cell}}}. \tag{5}$$

Therefore, we obtained the total cell ASR values according to Eq. (5) (Fig. 5e) and the proportions of the ohmic ASR (Fig. 5f). When the concentration polarization becomes significant at low SOCs during discharging and high current densities, the ohmic resistance still contributes 47.9%–61.4% to the cell resistance. More specifically, at 10% SOC and 121.7 mA·cm^{-2}, the ohmic resistance accounts for 47.9%, whereas at 100% SOC and 198.4 mA·cm^{-2}, the ohmic resistance is responsible for 61.4%.

The OCV, P_{max}, ohmic resistance, ohmic resistance proportion, and corresponding current density are summarized in Table 1. The ohmic resistance dominates the cell resistance at various states of the cell. According to Eq. (5), if the ohmic

CSTR: 32290.14.JUSTC-2024-0129
DOI: 10.52396/JUSTC-2024-0129
JUSTC, **2025**, 55(6): 0603

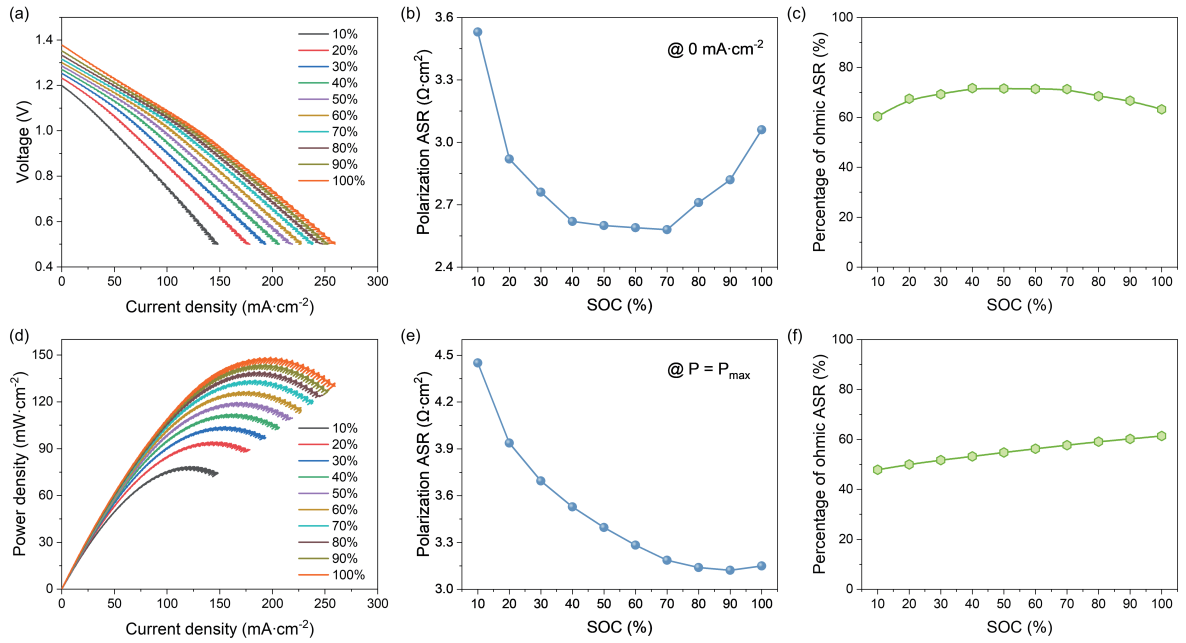

Fig. 5. (a) Cell potential versus discharge current density, (b) polarization ASRs at 0 mA·cm^{-2}, (c) percentages of ohmic ASR at 0 mA·cm^{-2}, (d) power density versus discharge current density, (e) polarization ASRs at the maximum power density, and (f) percentages of ohmic ASR at the maximum power density of the TEMPTMA/MV cell at various SOCs.

Table 1. Comprehensive EIS studies and cell polarizations of the TEMPTMA/MV cell assembled with a commercial AMVN membrane.

SOC (%)	OCV (V)	P_{max} (mW·cm^{-2})	Ohmic ASR (Ω·cm^2)	Percentage of ohmic resistance at 0 mA·cm^{-2} (%)	Percentage of ohmic resistance at $P = P_{max}$ (%)	Current density at $P = P_{max}$ (mA·cm^{-2})
10	1.183	78.62	2.130	60.3	47.9	121.7
20	1.219	94.35	1.970	67.5	50.0	142.9
30	1.241	104.21	1.912	69.3	51.7	155.5
40	1.259	112.31	1.879	71.7	53.3	166.1
50	1.275	119.68	1.861	71.6	54.8	165.9
60	1.290	126.72	1.848	71.4	56.3	177.9
70	1.306	133.83	1.839	71.3	57.7	183.6
80	1.323	139.37	1.856	68.5	59.1	188.0
90	1.342	144.20	1.880	66.7	60.2	193.7
100	1.368	148.52	1.933	63.2	61.4	198.4

resistance accounts for 60% of the cell resistance and is reduced by half, the maximum power density will be 1.4 times the original value. A membrane with lower resistivity may achieve this improvement after the electrolyte and electrode resistances are optimized.

4 Conclusions

Promoting the power output of AORFBs can lower stack costs to reach a target power density by reducing the area needed for expensive electrode and membrane components. We highlighted the dominance of the ohmic resistance in the total cell resistance at various states of the cell, as exemplified with the representative TEMPTMA/MV cell assembled with a commercial AMVN membrane. In this cell, the ohmic resistance is responsible for 60.3%–71.7% of the resistance of the entire cell at 0 mA·cm^{-2}, whereas the ohmic resistance still contributes 47.9%–61.4% when the power density reaches the maximum. The quantitative derivation of the maximum power density suggested that a membrane with lower resistivity may achieve an improvement in power performance. Our results provide insight into the development of high-power-density AORFBs.

Acknowledgements

This work was supported by the National Natural Science Foundation of China (22308345), the Anhui Provincial Natural Science Foundation (2308085QB68), and the Fundamental Research Funds for the Central Universities (WK2060000059).

CSTR: 32290.14.JUSTC-2024-0129
DOI: 10.52396/JUSTC-2024-0129
JUSTC, **2025**, 55(6): 0603

Conflict of interest

The authors declare that they have no conflict of interest.

Biographies

Kang Peng is currently a Specially-Appointed Associate Research Fellow at the University of Science and Technology of China (USTC). He received his B.E. and Ph.D. degrees from USTC in 2014 and 2019, respectively. His research mainly focuses on electrolytes and membranes of aqueous organic redox flow batteries.

Zhengjin Yang is a Professor at the University of Science and Technology of China. He received his Ph.D. degree from Tsinghua University in 2014. His research interests include aqueous organic redox flow batteries, polymers of intrinsic microporosity, confined mass transfer, and membranes for advanced separations.

References

[1] Arora N, Dar M I, Hinderhofer A, et al. Perovskite solar cells with CuSCN hole extraction layers yield stabilized efficiencies greater than 20%. *Science*, **2017**, *358*: 768–771.

[2] Yang W S, Park B W, Jung E H, et al. Iodide management in formamidinium-lead-halide–based perovskite layers for efficient solar cells. *Science*, **2017**, *356*: 1376–1379.

[3] Zhao Z M, Liu X H, Zhang M Q, et al. Development of flow battery technologies using the principles of sustainable chemistry. *Chemical Society Reviews*, **2023**, *52*: 6031–6074.

[4] Dunn B, Kamath H, Tarascon J M. Electrical energy storage for the grid: A battery of choices. *Science*, **2011**, *334*: 928–935.

[5] Haegel N M, Atwater H Jr, Barnes T, et al. Terawatt-scale photovoltaics: Transform global energy. *Science*, **2019**, *364*: 836–838.

[6] Zhu F L, Guo W, Fu Y Z. Functional materials for aqueous redox flow batteries: merits and applications. *Chemical Society Reviews*, **2023**, *52*: 8410–8446.

[7] Zhao Z M, Zhang C K, Li X F. Opportunities and challenges of organic flow battery for electrochemical energy storage technology. *Journal of Energy Chemistry*, **2022**, *67*: 621–639.

[8] Poizot P, Gaubicher J, Renault S, et al. Opportunities and challenges for organic electrodes in electrochemical energy storage. *Chemical Reviews*, **2020**, *120*: 6490–6557.

[9] Huskinson B, Marshak M P, Suh C, et al. A metal-free organic–inorganic aqueous flow battery. *Nature*, **2014**, *505*: 195–198.

[10] Lin K, Chen Q, Gerhardt M R, et al. Alkaline quinone flow battery. *Science*, **2015**, *349*: 1529–1532.

[11] Zhang L, Feng R, Wang W, et al. Emerging chemistries and molecular designs for flow batteries. *Nature Reviews Chemistry*, **2022**, *6*: 524–543.

[12] Amini K, Shocron A N, Suss M E, et al. Pathways to high-power-density redox flow batteries. *ACS Energy Letters*, **2023**, *8*: 3526–3535.

[13] Gao M, Salla M, Song Y, et al. High-power near-neutral aqueous all organic redox flow battery enabled with a pair of anionic redox species. *Angewandte Chemie International Edition*, **2022**, *61*: e202208223.

[14] Chen H N, Cong G T, Lu Y C. Recent progress in organic redox flow batteries: Active materials, electrolytes and membranes. *Journal of Energy Chemistry*, **2018**, *27*: 1304–1325.

[15] Zuo P P, Ye C C, Jiao Z R, et al. Near-frictionless ion transport within triazine framework membranes. *Nature*, **2023**, *617*: 299–305.

[16] Ji Y, Goulet M A, Pollack D A, et al. A phosphonate-functionalized quinone redox flow battery at near-neutral pH with record capacity retention rate. *Advanced Energy Materials*, **2019**, *9*: 1900039.

[17] Sun P, Liu Y H, Li Y Y, et al. 110th anniversary: Unleashing the full potential of quinones for high performance aqueous organic flow battery. *Industrial & Engineering Chemistry Research*, **2019**, *58*: 3994–3999.

[18] Peng K, Li Y Y, Tang G G, et al. Solvation regulation to mitigate the decomposition of 2,6-dihydroxyanthraquinone in aqueous organic redox flow batteries. *Energy & Environmental Science*, **2023**, *16*: 430–437.

[19] Peng K, Tang G G, Zhang C, et al. Progress and prospects of pH-neutral aqueous organic redox flow batteries: Electrolytes and membranes. *Journal of Energy Chemistry*, **2024**, *96*: 89–109.

[20] Tsehaye M T, Mourouga G, Schmidt T J, et al. Towards optimized membranes for aqueous organic redox flow batteries: Correlation between membrane properties and cell performance. *Renewable and Sustainable Energy Reviews*, **2023**, *173*: 113059.

[21] Janoschka T, Martin N, Hager M D, et al. An aqueous redox-flow battery with high capacity and power: The TEMPTMA/MV system. *Angewandte Chemie International Edition*, **2016**, *55*: 14427–14430.

[22] Mourouga G, Schaerer R P, Yang X, et al. Physics-based 0D-U-I-SoC cell performance model for aqueous organic redox flow batteries. *Electrochimica Acta*, **2022**, *415*: 140185.

[23] Wu M, Bahari M, Jing Y, et al. Highly stable, low redox potential quinone for aqueous flow batteries. *Batteries & Supercaps*, **2022**, *5*: e202200009.

[24] Huang J H, Hu S Z, Yuan X Z, et al. Radical stabilization of a tripyridinium–triazine molecule enables reversible storage of mMultiple electrons. *Angewandte Chemie International Edition*, **2021**, *60*: 20921–20925.

[25] Yuan X Z, Huang M B, Liang Z X. Effect of variable viscosity of electrolytes on mass transport and electrochemical reactions in aqueous organic redox flow battery. *International Journal of Heat and Mass Transfer*, **2023**, *205*: 123924.

[26] Pan L M, Sun J, Qi H H, et al. Dead-zone-compensated design as general method of flow field optimization for redox flow batteries. *Proceedings of the National Academy of Sciences of the United States of America*, **2023**, *120*: e2305572120.

[27] Aaron D, Tang Z, Papandrew A B, et al. Polarization curve analysis of all-vanadium redox flow batteries. *Journal of Applied Electrochemistry*, **2011**, *41*: 1175–1182.

[28] Esan O C, Shi X, Pan Z, et al. Modeling and simulation of flow batteries. *Advanced Energy Materials*, **2020**, *10*: 2000758.

[29] Zheng Q, Xing F, Li X F, et al. Flow field design and optimization based on the mass transport polarization regulation in a flow-through type vanadium flow battery. *Journal of Power Sources*, **2016**, *324*: 402–411.

CSTR: 32290.14.JUSTC-2024-0129
DOI: 10.52396/JUSTC-2024-0129
JUSTC, **2025**, 55(6): 0603